

# Battery State-of-Charge Approximation for Energy Harvesting Embedded Systems

Bernhard Buchli, Daniel Aschwanden, Jan Beutel

Computer Engineering and Networks Laboratory, ETH Zurich, Zurich, Switzerland  
{bbuchli, asdaniel, janbeutel}@ethz.ch

**Abstract** Batteries play an integral role in Wireless Sensor Networks as they provide the energy necessary to operate the individual sensor nodes. In order to extend the network's lifetime, and theoretically permit continuous operation even for systems with high-energy consumption, environmental energy harvesting has attracted much interest. It has been shown that the motes' utility can be improved significantly if run-time knowledge of remaining battery capacity is available. In this work, a light-weight and cost effective approach to approximating the battery state-of-charge (*SOC*) based on voltage measurements is presented. Despite commonly perceived as inferior to other approaches, a performance evaluation shows that *SOC* approximations with over 95% accuracy are possible. It is further shown that battery inefficiencies due to *e.g.*, temperature and aging are taken into consideration despite not explicitly modeling these effects. The approach only requires system input voltage measurements, but benefits from optional current and temperature measurements.

**Keywords:** Wireless sensor networks; battery state-of-charge; modeling; experimentation.

## 1 Introduction

Batteries play an important role in Wireless Sensor Networks (WSN), which are often deployed at remote locations, *e.g.*, [14], and can therefore not rely on power sources other than batteries. The battery's task is to provide the energy required to operate the WSN motes over extended periods of time. Once the battery is depleted, the sensor node's lifetime has expired, and its battery must be replaced. However, battery replacement can be a time consuming and costly endeavor. Hence, it is imperative that the batteries are reliable and capable of providing the energy necessary to operate the WSN motes according to requirements. Unfortunately, primary batteries can store only limited energy, which is inversely proportional to system lifetime. Particularly for high-energy consumers, the finite energy store imposes reduced utility due to limited runtime. For this reason, rechargeable batteries, supplemented with one of various types of environmental energy harvesting have attracted much interest in WSN scenarios [12, 16].

In outdoor WSN deployments, solar energy harvesting with photo-voltaic (PV) energy transducers is most commonly employed. There are a number of reasons for the prevalence of solar energy harvesting. First, solar panels achieve a high energy density,

even in indoor scenarios [27]. Low-cost commercial availability and relatively high conversion efficiency [15], reliability, and a periodically recurring energy source – the sun – are further contributing success factors. The cyclic behavior of the sun guarantees periodic opportunities for recharging the batteries. In theory, this enables perpetual system operation, which eliminates the need for periodic and costly battery replacement trips.

It has been shown that awareness of the energy available to the individual motes [21], and the entire network [7] can significantly improve overall system lifetime and utility. However, accurately determining the battery fill level, referred to as battery State-of-Charge (*SOC*), presents a non-trivial task. This is because a battery's *SOC* depends on many battery internal and external factors, such as size and type of battery, the rate at which it is discharged, as well as temperature and battery condition (*e.g.*, age, present *SOC*). While knowledge of the *SOC* may not be mission-critical for some WSN applications, improved observability, predictability, and utility [22, 29] may outweigh the efforts in implementing the necessary functionality.

As discussed in *Section 2*, many existing approaches to determine a battery's *SOC* depend on dedicated hardware to monitor the energy flux into and out of the battery. However, addition of special purpose hardware not only increases design complexity but also system cost [11]. Furthermore, upgrading existing systems with the hardware necessary may not be practical or even possible. Other approaches use complex models that incorporate the non-linear characteristics of batteries under varying and uncontrollable conditions. However, many of the proposed models present significant configuration and computational overhead [28]. Considering the limited computing resources on typical WSN platforms, these models may thus not be feasible for implementation.

This paper presents a practical trace-based, direct-measurement [3] method for on-line battery *SOC* approximation. It is aimed at systems with high energy demands that rely on off-the-shelf photo-voltaic (PV) harvesting components. The proposed approach does not need special purpose hardware, but only requires low-cost sensors that are commonly available on WSN platforms for system health monitoring. The method is computationally inexpensive as it does not depend on complex battery models. Instead, known characteristics of the PV system and the battery's behavior are leveraged.

The contributions of this paper can be summarized as follows. First, a computationally inexpensive, direct-measurement based method for on-line battery *SOC* approximation for energy harvesting systems is presented. Second, the proposed method's performance is evaluated with a proof-of-concept implementation, and experimental results are presented. Despite commonly perceived as inferior [24], it is shown that the direct-measurement approach achieves *SOC* approximation with an average error below 5% when compared to discharge tests. Furthermore, accurate lifetime predictions even with temperature fluctuations and varying battery, and load conditions are possible as the method implicitly accounts for battery inefficiencies like temperature and aging.

The remainder of this paper is structured as follows. *Section 2* discusses common approaches to battery *SOC* determination, and adaptations to WSN scenarios. *Section 3* provides an overview of the system architecture and battery characteristics that form the foundation of the proposed approach. *Section 4* then discusses the *SOC* approximation in detail. *Section 5* describes the experimental set-up and presents a performance evaluation of the approach. Finally, *Section 6* presents the concluding remarks.

## 2 Review of Battery State-of-Charge Approximation

Efforts to estimate the residual charge contained in a battery have been made for almost as long as rechargeable batteries exist, and increasing popularity of hybrid electric vehicles has further pushed this research topic. Hence, literature review reveals a host of battery state-of-charge (*SOC*) approximation models, of which common techniques are presented in this section. A brief review of WSN specific approaches is also provided.

**State-of-Charge Determination Methods.** One of the earliest approaches is in the form of current integration, usually referred to as coulomb counting [24, 25]. With this approach, charge flowing from (in case of discharging), or to the battery (charging) is measured and integrated over time. After subtracting the net charge from a full battery, the residual charge contained in the battery can be obtained. Although widely used today, this approach suffers from a number of issues. First, to yield acceptable accuracy, battery inefficiencies that are not directly measurable must be compensated for. Second, inaccurate current readings lead to an accumulation of error, but accurate current measurements are expensive, and the addition of the necessary hardware can add substantial design complexity and development cost. Finally, since the performance depends on known initial conditions, regular re-calibrations are required [24, 25].

A technique that attempts to improve the performance of coulomb counting is called book-keeping [3]. With this approach, common battery inefficiencies, such as discharging efficiency, self-discharge, and capacity loss are taken into consideration to yield a more accurate *SOC* indication. These inefficiencies, and details on how the model proposed in this paper copes with their effects are discussed in *Section 5*.

A discharge test under controlled conditions is considered to be the most reliable means of approximating a battery's *SOC* [24], and commonly performed by the battery manufacturer [9]. For this reason, results from discharge tests are used as ground-truth for the evaluation of the proposed *SOC* approximation method. Nevertheless, discharge test are not feasible for most if not all practical applications because system operation is interrupted willingly and possibly for long periods of time.

Another technique that is applicable to vented lead-acid (LA) batteries with liquid electrolytes is in the form of measuring the electrolytes' physical properties. LA batteries, which are common in cars and stationary photo-voltaic energy harvesting systems, exhibit a relationship between the electrolyte's properties and *SOC*. Therefore, by measuring *e.g.*, specific gravity, conductivity, and ion-concentration, the battery's *SOC* can be determined. However, to obtain an accurate *SOC* indication, the temperature must be considered, and measurements may only be taken after a proper charging cycle and appropriate resting period of the battery. This, together with the need for measuring the battery's internal properties limit the applicability of this approach.

A lead-acid battery's electrolytes' properties are also directly related to the open-circuit voltage. Hence, the battery's *SOC* can be obtained by measuring the battery's terminal voltage when no load is connected. However, this necessitates periodic load disconnects, which requires special design considerations. Just like with the previous approach, appropriate resting times are required to obtain meaningful measurements.

Recently, there has been significant efforts in devising analytic models for batteries and *SOC* determination. An excellent review is given in [28]. These models range from electrical circuit equivalents, over stochastic load modeling, to mixed models that incor-

porate both experimental data and physical laws. In particular, extended [30], and adaptive [13] Kalman filtering techniques have emerged. Unfortunately, these approaches require significant configuration efforts and exhibit computational complexity that preclude application in low-performance systems such as WSN motes [28].

Finally, the approach most closely related to the one discussed in this work consists of direct voltage measurements [25]. Voltage measurements are generally considered to yield inaccurate *SOC* indication because a battery's voltage profile depends on discharge rate, temperature effects, and age of the battery to name a few. However, as will be elaborated in the remainder of this work, if the battery's behavior under load, and the discharge current are known (or measurable), the *SOC* can be obtained with good accuracy even under varying battery operating conditions.

**State-of-Charge Determination in WSN Scenarios.** Of the approaches discussed so far, only a subset is feasible for implementation in WSN scenarios. This may be due to cost considerations, physical constraints, and limited processing power available on the motes. In addition to special-purpose hardware [17, 26], fully software [8, 11, 18] based approaches to *SOC* determination have been proposed, and are briefly introduced here.

In [8] a software based *SOC* model for lifetime prediction is presented. The platform load is characterized by a constant average current for each activity (*i.e.*, sensing, processing, and transmission). The *SOC* is then approximated in software by “counting” the charge over the period of time a given component is active. The authors report a lifetime estimation error below 10%. However, their approach requires current measurements of the PV system or, alternatively a light meter. Both require pre-deployment design considerations, which precludes its use in existing systems.

Although not aimed at energy harvesting systems, [11] and [18] follow a similar approach. Software routines are implemented that are executed every time a certain hardware component is switched on or off. The total time a given component is active is then multiplied by its average current drain, which is obtained by pre-deployment power profiling of the system. Finally, to obtain the overall system energy consumption (and hence infer the battery *SOC*), all components are summed up. It is not clear what accuracy either of these approaches achieves, but considering that coulomb counting integrated circuits (ICs) require frequent re-calibration, it can be assumed that the error in purely software counting techniques accumulates just as rapidly.

In contrast to purely software based approaches, [26] presents Heliomote, a custom energy harvesting hardware module as add-on for Berkley/Crossbow motes. It is a complete power management solution that autonomously controls solar harvesting, charging of the battery, storage and power routing, and provides harvesting and battery state information to the host platform. While not exclusively aimed at providing *SOC*, the authors show that harvesting aware power management can improve system utility.

Similarly, SPOT [17] is another application specific custom micro power meter for energy monitoring of MicaZ motes. As motivation, the authors state that commercially available ICs are not designed to meet WSN application requirements. Similar to Heliomote, the immediate aim is not battery *SOC* determination, but rather empirical on-site evaluation of low power designs at scale. A price tag of \$25 is stated, but it is not clear how much re-design and integration effort would be necessary to adapt the SPOT module to other mote platforms.

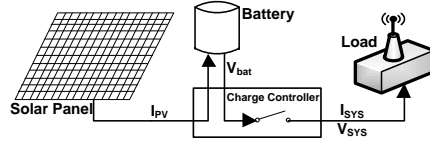


Figure 1: System architecture with off-the-shelf energy harvesting components (solar panel, battery, charge controller), and load.  $I_{sys}$  and  $V_{sys}$  are assumed to be observable.

### 3 System Concept

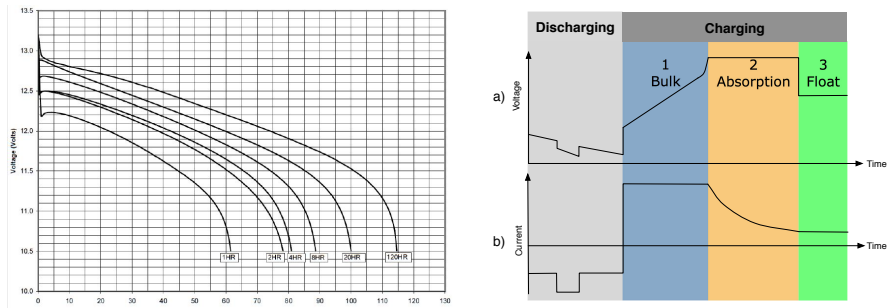
**System Architecture and Assumptions.** For the proof-of-concept implementation discussed in this paper, an off-the-shelf (OTS) energy harvesting set-up depicted in *Figure 1* is assumed. It consists of an energy harvesting module, such as a solar panel, a PWM charge controller [20], and one or multiple Valve Regulated-Absorbent Glass Mat (VR-AGM) sealed lead-acid batteries [9]. While this is not a typical set-up for low-power motes with simple sense-and-transmit applications it can be considered a reasonable, low-cost set-up for systems with high-energy consumption due to high-power sensors and increased duty-cycles. Aside from WSN basestations [14] that usually have considerable energy demands, recently proposed application scenarios like continuous GPS [6], acoustic emission [31], or Audio/Video surveillance [2] validate such a set-up.

With an OTS set-up, the charge controller regulates proper charging of the battery, but does not provide *SOC* information. Therefore, the proposed approach aims at approximating the *SOC* in a battery type, and set-up independent manner. The goal is to provide a solution that does not depend on extensive hardware support, but gets by with low-cost sensors commonly available on contemporary WSN motes. Furthermore, accurate *SOC* indication should be possible without requiring extensive processing.

Although a lead-acid (LA) battery chemistry is assumed in this work, the approach is expected to apply to any battery chemistry with an appropriate discharge profile. The model is agnostic to a particular set-up and harvesting source, and only requires a well-defined behavior of the charge-controller and the battery behavior under load.

**Battery Model.** Devising an analytic battery model that takes into consideration all the battery's non-linearities has proven to be complex [3] and, depending on application, computationally prohibitively expensive [28]. However, incorporating all inefficiencies into the model may not be necessary for achieving acceptable *SOC* approximation. Instead, from the illustration of a battery's voltage profile (obtained from its data-sheet [9]) in *Figure 2a* it is observed that a battery exhibits qualitatively very similar voltage versus Depth-of-Discharge (*DoD*) curves for different discharge rates (*DoD* is the complement of *SOC*). The battery's charging and discharging characteristics are explained in the following. *Section 4* then explains how these characteristics are leveraged to obtain information on the battery's state-of-charge.

**Capacity and Cut-off Voltage.** The manufacturer provided capacity rating specifies the battery's nominal capacity, which refers to the maximum charge that can be withdrawn before fully depleting the battery (*i.e.*, 100% *DoD*) at a specified discharge rate and temperature. Usually, the discharge rate and temperature are assumed to be  $C/20$  and  $25^\circ\text{C}$ , which means that the battery is fully discharged in 20 hours. However, since deep discharge cycles cause irreversible chemical reactions, the battery should not be



(a) Manufacturer provided Depth-of-Discharge (*DoD*) versus terminal voltage [9] for 1, 2, 4, 8, 20, and 120-hour discharge rate (as a percentage of 20-hour rate) of a VR-AGM battery. (b) Relation between battery terminal voltage (top) and current (bottom) during the charging and discharging processes.

Figure 2: (a) Battery discharge profile at different discharge rates, and (b) qualitative illustration of battery behavior during charging and discharging processes.

fully discharged. To protect the battery and maximize its lifetime, commercial charge controllers therefore implement a cut-off voltage, below which the load is disconnected until the battery recovers to a certain *SOC* (usually 60% of nominal capacity).

The known cut-off voltage provides two pieces of information that are leveraged in the proposed model. First, the cut-off voltage is used to define the 0% *SOC* (or 100% *DoD*) of the battery. Second, since this voltage is set such that it limits the *DoD* to 20%, it can be assumed that the battery can deliver 80% of the nominal capacity. This assumption has been experimentally verified with a coulomb counter [19] in *Section 5*.

**Charge and Discharge Profiles.** The behavior of a battery can be classified into two processes: charging and discharging. The charging process can be further segmented into three phases: Bulk, Absorption, and Float charging. These processes are illustrated in *Figure 2b* and briefly explained in the following. For simplicity, ideal conditions – that is no charging inefficiencies, and a stable power source – are assumed.

**Discharging.** The battery is discharged with a certain drain current that defines the rate of discharge. Electro-chemical reactions lead to an increase in battery internal resistance, which causes a drop of the battery’s terminal voltage directly related to the magnitude of the drain current, as illustrated in *Figure 2a*.

**Bulk Charging.** In this phase, a constant current is applied, which causes the battery potential to increase until a preset, temperature dependent voltage is reached. The time for reaching this voltage depends on the magnitude of the drain current and the battery’s *SOC* at the beginning of the charging process.

**Absorption Charging.** In this phase the voltage is kept at a constant voltage level defined by the bulk phase. The charging current is tapered off until it drops below a certain percentage of the battery’s nominal capacity (0.5% for the batteries used [9]), after which the battery can be considered fully charged.

**Float Charging.** The final charging phase attempts to keep the battery at 100% *SOC*. To prevent overcharge, the voltage is reduced to a temperature dependent float volt-

age and the charging current is kept constant. Depending on the present *SOC*, and the magnitude of the charging and drain currents, this phase may not be reached.

## 4 State-of-Charge Approximation

This section develops a set of equations that can be used to obtain harvesting source, and set-up independent indication of residual charge stored in the battery.

### 4.1 Discharge Approximation

To model the behavior of the battery under varying loads, a three step procedure is performed to extract the necessary information. The following explains the procedure for the discharging process. *Section 4.2* then elaborates on the charging process.

**Trace Generation.** A trace consists of fixed interval measurements of the battery voltage and system drain current until the battery is fully drained. The magnitude of drain currents should be chosen such that the traces bound the expected operational range of the system. An illustration of discharge traces at various rates is shown in *Figure 2a*. Since the data provided by the manufacturer is for rates much higher than required, the battery is profiled with discharge rates appropriate for the particular system [5] used.

**Trace Transformation.** Next, a domain transformation of the traces from the time domain to Depth-of-Discharge (*DoD*) domain is performed, which is defined for the interval  $[0,1]$ . To this end, the known cut-off voltage of the charge controller is leveraged to define 100% *DoD*. The known battery voltage of a fully charged battery defines 0% *DoD*. Using the recorded time  $t_{cutoff}$  it takes the battery to reach the cut-off voltage, the *DoD* is assigned linearly in time ( $DoD(t) = t/t_{cutoff}$ ). Finally, the traces are inverted to obtain *DoD* as a function of battery voltage.

**Coefficient Extraction.** After transformation of the traces, the battery voltage dependent *DoD* can now be approximated with a polynomial function of order  $n$  (*Equation (1)*). The choice of  $n$  is a trade-off between computational complexity and fitness of the traces, but it has been found that a quadratic approximation achieves good results (see *Section 5*). Since the coefficients  $a_n$  vary with the load, they depend on the discharge current. Rather than using the absolute drain current, it is noted that the load caused by the drain current is relative to the nominal capacity of the battery. For this reason, the relative load (RL) is introduced, which normalizes the discharge current  $I_{sys}$  with respect to the battery's nominal capacity  $C_{bat}$ , and is defined as  $RL = I_{sys}/C_{bat}$ . Thus, the *DoD* approximation for trace  $i$  is defined by *Equation (1)*.

$$\widehat{DoD}_i(V_{bat}, RL) = a_{i,n}(RL) \cdot V_{bat}^n + a_{i,n-1}(RL) \cdot V_{bat}^{n-1} + \dots + a_{i,1}(RL) \cdot V_{bat} + a_{i,0}(RL) \quad (1)$$

It is desirable to obtain a single *DoD* equation that covers the entire operating range, including relative loads other than the ones recorded. Therefore, to obtain the coefficients  $a(RL)$  in *Equation (1)*, another set of polynomial approximations of order  $m$  is performed over all trace coefficients  $a_{i,n}$  to find the coefficients  $b_{n,m}$  in *Equation (2)*. The end result is a single equation representing the *DoD* as a function of relative load and battery voltage, and  $n + 1$  equations for the the coefficients  $a_n$  (*Equation (2)*).

$$a_n(RL) = b_{n,m} \cdot RL^m + b_{n,m-1} \cdot RL^{m-1} + \dots + b_{n,1} \cdot RL + b_{n,0}, \quad m \geq n \quad (2)$$

## 4.2 Charge Approximation

To obtain a model for the *SOC* approximation during the charging process, a procedure similar to the one discussed in *Section 4.1* is followed. However, as an off-the-shelf set-up is assumed, the charging current,  $I_{PV}$ , produced by the solar panel cannot be measured directly and must therefore be approximated. This is necessary because, depending on the magnitude of  $I_{PV}$ , and assuming non-zero drain current  $I_{sys}$ , the resulting charge ( $I_{bulk}$ ,  $I_{abs}$ ) flowing into the battery may be positive or negative.

**Bulk Approximation.** In the ideal case, the bulk charging current,  $I_{bulk} \leq I_{PV}$ , flowing into the battery is constant, causing the voltage to increase monotonically. The relative charging current,  $\widehat{RC}_{bulk} = I_{bulk}/C_{bat}$  is used to determine the current *SOC* during the bulk phase in a conservative way (conservative because the current is relative to nominal, rather than actual capacity). If charging inefficiencies are ignored for the moment, this increase is relative to the previous *SOC*. Hence the *SOC* is computed using *Equation (3)*, where  $t_{bulk}$  represents the time elapsed since the last update.

$$\widehat{SoC}(t) = \widehat{SoC}(t - t_{bulk}) + \widehat{RC}_{bulk} \cdot t_{bulk} \quad (3)$$

However, the exact value for  $I_{bulk}$  is unknown, and  $\widehat{RC}_{bulk}$  must therefore be approximated. Fortunately, the rate at which the voltage increases during the bulk phase is directly proportional to  $\widehat{RC}_{bulk}$ . Therefore, the slope  $\frac{\delta V}{\delta t}$  of the trace is approximated by a linear regression. Since the traces are collected with known relative charging current, the corresponding slopes of the voltage profiles are used to extract the coefficients  $c_0$  and  $c_1$  of the first order approximation of  $\widehat{RC}_{bulk}$ , shown in *Equation (4)*.

$$\widehat{RC}_{bulk} = c_1 \cdot \frac{\delta V}{\delta t} + c_0 \quad (4)$$

**Absorption Approximation.** As explained in *Section 3*, the absorption phase is characterized by an exponentially decreasing charging current with initial value given by  $\widehat{I}_{bulk}$ . Due to constant terminal voltage during this phase,  $I_{abs}$  cannot be approximated by the voltage in the same way it is done for bulk charging. Since it is assumed that the charging current  $I_{PV}$  cannot be measured, one option to approximate the relative charge  $\widehat{RC}_{abs}$  is by considering the known behavior of  $I_{abs}$ . For this an ideal scenario is assumed, *i.e.*, the current source does not fluctuate significantly.

Therefore,  $\widehat{RC}_{abs}$  is approximated with *Equation (5)*, where  $\widehat{\lambda}$  is the decay constant, which is dependent on the relative charging current during the bulk phase. The true decay constant  $\lambda$  is found by an exponential fit of the corresponding charging traces. Then, as *Equation (6)* shows,  $\widehat{\lambda}$  is approximated by a linear interpolation of the relative charging current  $\widehat{RC}_{bulk}$ . The coefficients  $d_1$  and  $d_0$  are obtained by a linear regression of  $\lambda$  and  $\widehat{RC}_{bulk}$  for each trace. Finally, since the relative charging current  $\widehat{RC}_{abs}$  is decreasing over time, the *SOC* is updated differentially for each discrete time step  $\Delta t$  (*Equation (7)*). *Equation (5)* can be approximated by a Taylor series if need be.

$$\widehat{RC}_{abs}(t) = \widehat{RC}_{bulk} \cdot e^{(\widehat{\lambda}(\widehat{RC}_{bulk}) \cdot t_{abs})} \quad (5)$$

$$\widehat{\lambda}(\widehat{RC}_{bulk}) = d_1 \cdot \widehat{RC}_{bulk} + d_0 \quad (6)$$

$$\widehat{SoC}(t) = \widehat{SoC}(t - \Delta t) + \widehat{RC}_{abs}(t) \cdot \Delta t \quad (7)$$

**Float Approximation.** The *SOC* of the float phase is by definition 100%. This phase can easily be detected by the float voltage given in the battery’s data-sheet [9].

### 4.3 Battery State Tracking

For tracking the behavior of the battery over time, a Finite-State Machine (FSM) is defined. The FSM’s states correspond to the 4 charge and discharge phases explained in Sections 3 and 4.1. An additional UNKNOWN state is introduced to capture initial conditions. Figure 3 shows the states and transitions of the FSM used. The triggers for the individual state transitions are listed in Table 1.

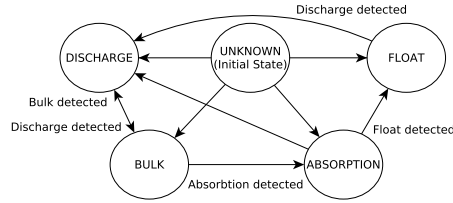


Figure 3: State Machine for charge/discharge tracking. Transitions are listed in Table 1

Table 1: State transition matrix.  $\uparrow$  and  $\downarrow$  refer to ‘increase’ and ‘decrease’, respectively, while  $\nearrow$  and  $\nwarrow$  refer to ‘no increase’ and ‘no decrease’ of the respective parameter.

		Next State				
		UNKNOWN	DISCHARGE	BULK	ABSORPTION	FLOAT
Current State	UNKNOWN	No change	$V \downarrow, I_{sys} \nearrow$	$V \uparrow, I_{sys} \nwarrow$	$V \geq V_{abs}$	$V \geq V_{float}$
	DISCHARGE	–	No change	$V \uparrow, I_{sys} \nwarrow$	$V \geq V_{abs}$	$V \geq V_{float}$
	BULK	–	$V \downarrow$	No change	$V \geq V_{abs}$	$V \geq V_{float}$
	ABSORPTION	–	$V < V_{float}$	–	No change	$V_{float} \leq V < V_{abs}$
	FLOAT	–	$V < V_{float}$	–	–	No change

### 4.4 Measurement Considerations

The goal is to implement a light-weight HW/SW approach to battery *SOC* approximation that does not depend on special-purpose hardware. Nevertheless, since the approach relies on voltage measurements, at least a voltage sensor is required that can measure the unregulated system input voltage with sufficient resolution and accuracy. The drain current can be obtained by profiling, as is done in [8, 11, 18]. However, the instantaneous *SOC* approximation can be improved by employing a current sensor to measure the true system drain current. If the *SOC* should also be tracked during charging of the battery, a temperature sensor to measure the battery’s temperature must also be available because the charging process is temperature sensitive. These sensors are generally present on WSN motes for health monitoring, and are therefore not considered special-purpose hardware.

During discharging of the battery, the proposed algorithm is stateless and only considers the present measurements to compute the *SOC*. This means that the model’s

accuracy is independent of the sampling period, and the health measurements of the respective application can be conveniently re-used whenever they are scheduled anyway. This eliminates measurement overhead and reduces possible interference with normal system operation. However noise on the sensor readings may affect the solution quality. For this reason an exponentially weighted moving average (EWMA) filter with length 10 is used to smoothen all physical measurements.

For the charging process the output depends both on the present measurement and previous *SOC*. In this case it is clearly beneficial to use a sampling period appropriate to capture the dynamics of the energy source used. With solar harvesting the source tends to fluctuate slowly, so a sampling period of a few minutes can be considered sufficient.

With an off-the-shelf set-up assumed and depicted in *Figure 1*, the system input voltage does not correspond to the actual battery voltage. However, to approximate the *SOC* in a set-up independent manner, the battery's terminal voltage is required. Therefore, voltage drops caused by the charge controller and the power cable, or any other consumers must be explicitly accounted for. Finally, it is worth noting that for this algorithm no *SOC* updates can be made during sleep periods, unless supervisory circuit with the ability to read the sensors and execute the FSM introduced in *Section 4.3* is available.

## 5 Evaluation

This section presents the performance result of the proposed *SOC* approximation approach when used with an OTS power sub-system and high energy consumer, *e.g.*, WSN basestation [14] or applications with high-power sensors and increased duty-cycles [6].

### 5.1 Experimental Set-up

**Model Parameters.** In *Section 4* general equations for obtaining the *DoD* as a function of the battery voltage and relative load have been developed. *Table 3* list the respective coefficients, which have been found by fitting discharge traces of a single battery identical to *BAT1* (*Table 2a*) with relative loads of 0.00471, 0.01194, and 0.01638 with a quadratic approximation. A cubic fit was found not to improve the model's performance appreciably.

**Test Set-up.** For evaluating the proposed model, constant power discharge tests are carried out with three Absorbent Glass-Matt (AGM) batteries [9] listed in *Table 2a*. A custom platform of which details are given in [5], presents the load and executes the logic described in *Section 4* with the parameters shown in *Table 2b*. To verify that batteries of the same size yield the same results, a discharge test is performed on two identical batteries. The differences are found to be insignificant, hence only one set of results is presented in the following.

**Evaluation Baseline.** To validate the assumption about available battery capacity made in *Section 3*, an external coulomb counter [19] is placed between the charge controller and the battery. In order to evaluate the method's ability to adapt to conditions that are not explicitly modeled, such as varying size, condition, etc., a number of discharge tests are carried out and discussed in the following. Discharge tests under controlled conditions are considered to yield accurate indication of *SOC* [9, 24]. Before starting each test, the respective battery is fully charged and allowed to rest for 4 hours.

Table 2: (a) Type, capacity, and condition of the batteries [9] used, and (b) Sampling rate and filter specification for smoothing of physical measurements.

Name	Type	Capacity (C/20)	Condition	Description	Value
BAT0	GPL-1400T	43 Ah	Old	Sampling rate	30 sec.
BAT1	GPL-U1T	33 Ah	New	Filter type	EWMA
BAT2	GPL-1400T	43 Ah	New	Filter length	10

Table 3: Coefficients for *Equations* (2), (4), and (6) found by interpolation of traces.

Coeff.	Value	Coeff.	Value	Coeff.	Value	Coeff.	Value	Coeff.	Value
$b_{2,0}$	-8.321e-9	$b_{1,0}$	-0.07018	$b_{0,0}$	100	$c_0$	0.005573	$d_0$	-0.003891
$b_{2,1}$	-0.002257	$b_{1,1}$	4.492	$b_{0,1}$	0	$c_1$	1.296	$d_1$	-0.1091
$b_{2,2}$	0.08133	$b_{1,2}$	-204.7	$b_{0,2}$	0				

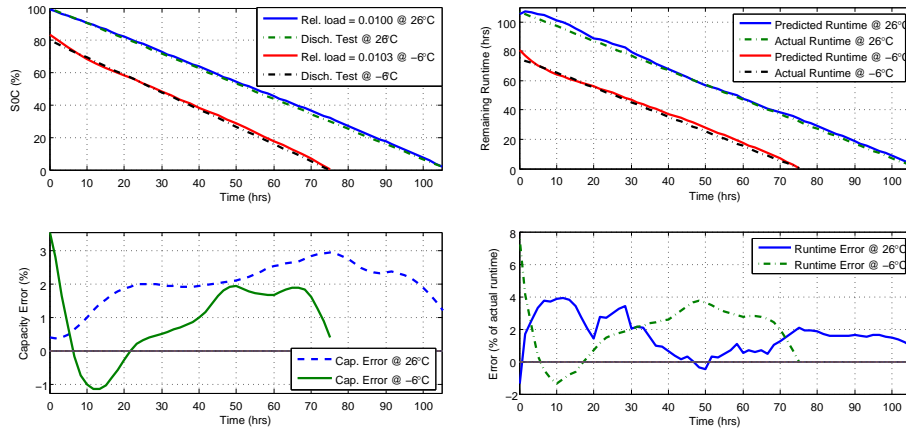
## 5.2 Experimental Results

In the discussion so far, battery inherent inefficiencies have been ignored. However, when operated under varying, and uncontrollable conditions, batteries exhibit nonlinearities that cannot be neglected. Therefore, the performance of the *SOC* approximation is first evaluated with a battery exposed to different temperatures. Then, the model’s ability to adapt to aging batteries is investigated. Finally, test results obtained with varying loads, and the model’s accuracy in predicting remaining runtime are presented. It is important to note that the goal is to evaluate the performance of the proposed approach, and *not* the battery behavior under the conditions mentioned.

**Temperature Effects.** Temperature variations have a strong impact on the battery’s *SOC* as they affect the apparent capacity [9, 28]. Low temperatures cause a reduction of the electrochemical activity, which leads to a (temporary) reduction of energy available (relative to the rating), and the opposite is true for high temperatures. Since the battery parameters were obtained at 22 °C, the first experiment evaluates the model’s ability to adapt to lower temperatures. To this end, *BAT1* is cooled down and kept at  $-6$  °C while being discharged with a constant average relative load of 0.0103. This specific temperature is selected as it represents a typical average temperature during winter months at a particular deployment location of interest [4]. *Figure 4* and *Table 4* show the results, which are briefly discussed in the following.

The upper graph in *Figure 4a* shows the *SOC* approximation of both the model and the ground-truth at constant  $-6$  °C, and for reference at 26 °C. The lower graph shows the capacity error, which is defined as  $SoC_{model} - SoC_{DT}$ , *i.e.*, the difference between the *SOC* indicated by the model and capacity inferred by the discharge test. At  $-6$  °C the maximum overestimate of 3.54% occurs only in the very beginning but quickly drops during the first 6 hours until reaching a maximum underestimate of  $-1.17\%$  after 12 hours. After 25 hours, and for the remainder of the test, the error varies between roughly 0.3% and 2% with a mean deviation from the ground-truth of 0.85%.

The reason for the initial overestimate is because of the increased rate at which the voltage drop occurs due to the low temperature. This causes the model to overestimate the *SOC* until the battery has adjusted to the load, at which point the rate of change in the voltage profile slows down and reflects the actual condition. The consistent overes-



(a) *SOC* approximation (top) and error (bottom). (b) Runtime prediction (top) and prediction error (bottom).

Figure 4: Constant power discharge test at constant  $26^{\circ}\text{C}$  and  $-6^{\circ}\text{C}$  with battery *BAT1*.

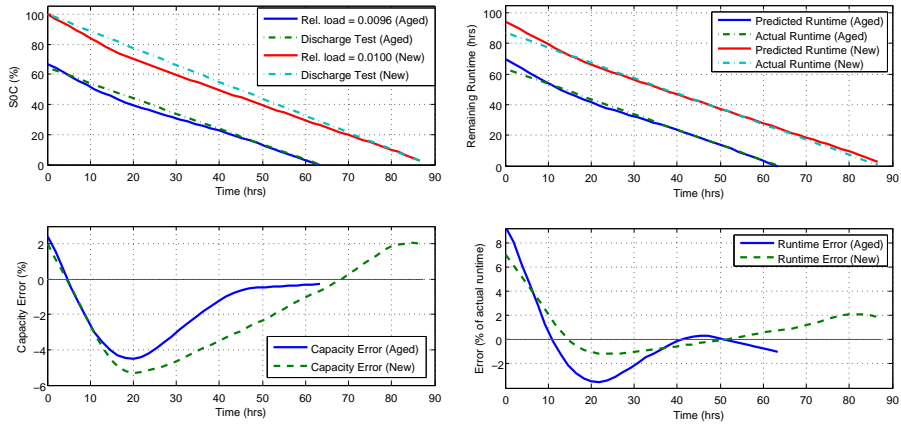
minate in both cases is likely due to considering too little voltage drop across the charge controller and cabling (see *Section 4.4*).

Another inefficiency that is highly temperature dependent and common to all batteries is referred to as self-discharge. This phenomenon causes the battery to discharge at a type and temperature specific rate [1] even with no load connected. This effect is ignored as it is assumed that an off-the-shelf charge controller presents a load that is always larger than the battery’s self-discharge.

In summary, the temperature, and – as will be shown in the following – aging effects are indirectly considered through changes in terminal voltage that occur due to temperature variations without a corresponding change in drain current. The change in voltage induced by these effects causes the model to yield a correspondingly lower or higher *SOC*. It is important to note that  $0\%$  *SOC* is not affected by temperature because the charge controller disconnects the load at a temperature independent cut-off voltage.

**Aging Effects.** Each charge/discharge cycle causes irreversible chemical reactions within the battery. This causes a gradual decrease in the maximum charge the battery can store and deliver [3], and is referred to as capacity loss. Conventionally, a battery has reached its end-of-life when it fails to store and deliver a certain percentage (usually  $80\%$ ) of its nominal capacity [9]. Since capacity and voltage are related [24], an old battery will exhibit a lower terminal voltage (compared to a new battery) due to lower electrochemical activity. Therefore, identically to temperature effects discussed previously, the model indirectly considers aging effects via its impact on terminal voltage.

*Figure 5* and *Table 4* show the results of the discharge test with *BAT0*, which has reached its end-of-life. For reference, the same discharge test is carried out with *BAT2*, which is of the same type, but in new condition. The initial capacity is determined using a coulomb counter, which indicates that only  $52\%$  of the nominal capacity (equivalent to roughly  $65\%$  of available capacity) can be withdrawn when *BAT0* is fully charged. As is evident from the top most graph in *Figure 5a*, this agrees very well with the initial *SOC* approximated by the model. The maximum and mean deviation from the ground-truth



(a) *SOC* approximation (top) and error (bottom). (b) Runtime prediction (top) and prediction error (bottom).

Figure 5: Discharge test with aged (*BAT0*), and new (*BAT2*) batteries.

of -4.49%, and -1.69% respectively may seem rather high. However, the negative values represent an underestimate, which is maintained almost over the entire range. This may be viewed as a conservative indication of *SOC*, and, depending on application, may even be desirable. It is worth noting that, except for in the beginning, both discharge tests yield very similar profiles, which validates the method’s applicability to varying battery conditions. Unfortunately, the model parameters, which are obtained with a battery size equivalent to *BAT1*, tend to introduce error when used with the larger batteries. The effect is visible for both cases by the trough shortly after starting the test.

**Load Variations.** Practical applications typically do not exhibit constant power dissipation, hence this section presents the model’s performance when exposed to varying drain currents. Load changes frequently occur in real systems, due to *e.g.*, duty-cycling. It is well known [10,23] that a battery behaves non-linearly when discharged at different rates. These rate dependent effects are known as rate-discharge, and recovery effects.

Figures 6 and 7 and Table 4 present the results of a discharge test with bimodal load changes. As illustrated in the lower graph in Figure 6, which shows the voltage profile, the high-power mode presents a maximum relative load of 0.0170 and is active 35% of the time, while the “low-power” mode presents a relative load of 0.0055 for the remaining 65%. In this discharge test, the rate discharge and recovery effects become visible. With variations in the load, the battery is allowed to recover some of the charge regularly. Unfortunately, the model tends to continuously fluctuate between under- and overestimating the *SOC*. Towards the end of the discharge test, the maximum overestimate reaches 4.98%. Nevertheless, despite the load changes and their visible effects on the voltage profile, the *SOC* exhibits a relatively linear tendency with a mean deviation from the expected value of 3.02%.

**Lifetime Estimation.** The ability to predict the remaining runtime is clearly more beneficial to the system than mere indication of battery *SOC*. For this reason, this section investigates if the approximated *SOC* can be used to easily predict remaining runtime. In addition to the instantaneous *SOC* and drain current, the manufacturer specified non-

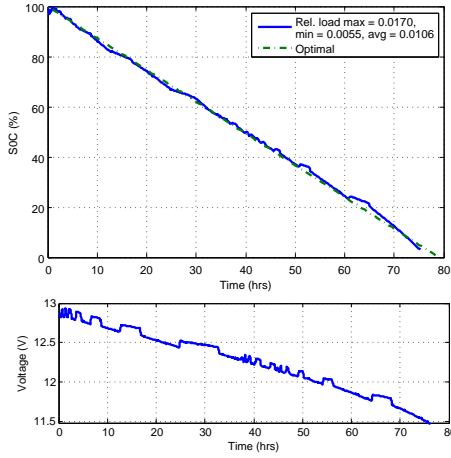


Figure 6: *SOC* approximation (top), and voltage profile (bottom) for bimodal load.

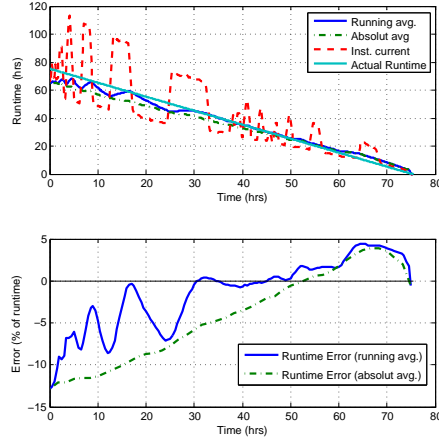


Figure 7: Runtime prediction (top) and prediction error (bottom) for bimodal load.

inal capacity  $C_{bat}$  in mAh is used as basis for computing the remaining lifetime  $L$ , as shown in Equation (8).

$$L(t) = SOC(t) \cdot \frac{C_{bat}}{I_{sys}(t)} \cdot \alpha \quad (8)$$

The scaling factor  $\alpha$  is required to account for rate-discharge and recovery effects with variable loads. Therefore, All but the experiment with varying loads use  $\alpha = 1$ . This implies that when the battery is discharged with the constant loads evaluated, the assumed capacity (*i.e.*, 80% of  $C_{bat}$ ) is actually available. In the more interesting case with varying loads, rate-discharge and recovery effects have an impact on the assumed capacity, which requires an appropriate scaling to yield acceptable lifetime prediction. For the results shown in Figure 7,  $\alpha = 0.7$  has been found to yield the lowest average lifetime prediction error.

As expected, however,  $\alpha$  does not behave linearly with the discharge duty-cycle. Another set of tests carried out with a duty-cycle of 50% and periods of one ( $\alpha = 0.85$ ), two ( $\alpha = 0.88$ ), and four hours ( $\alpha = 0.88$ ) verifies this. This illustrates the well known fact [3] that the rate at which the load varies affects the actually available charge in the battery. The implication is that for a simple lifetime prediction approach like Equation (8),  $\alpha$  may have to be learned on-line if the duty-cycle is not known in advance.

Another complication arises due to the current  $I_{sys}$  to compute the lifetime. This is illustrated in the upper graph in Figure 7, which shows the runtime predicted by the model. The smooth curve represents the lifetime with a running average for  $I_{sys}$ , while the dashed curve represents the prediction when using the instantaneous measured current instead. As is to be expected, in the latter case the prediction follows the voltage profile closely (which follows the drain current). In the former case, the averaging operation smoothens the prediction such that it follows the actual runtime much more closely. Depending on application, either of the approaches may be favorable.

Table 4b and the lower graph in Figure 7 show the prediction error for the running, and absolute average respectively. It would not be fair to compare the instantaneous

Table 4: Results of the *SOC* approximation performance shown in *Figures 4 – 7*.  
(a) Cap. error in % ( $SoC_{model} - SoC_{CC}$ ). (b) Lifetime error in % of actual runtime.

Test	Fig.	Max.	Min.	Mean	Var.	Std.	Test	Fig.	Max.	Min.	Mean	Var.	Std.	$\alpha$
26 °C	4a	2.98	0.33	2.0	0.44	0.66	26 °C	4b	3.85	-1.38	1.4	2.95	1.72	1.0
-6 °C	4a	3.54	-1.1	0.85	0.96	0.98	-6 °C	4b	7.54	-1.34	1.95	2.87	1.7	1.0
Aged	5a	2.41	-4.49	-1.69	3.24	1.8	Aged	5b	9.21	-3.52	-0.07	9.52	3.09	1.0
New	5a	2.04	-5.32	-1.81	5.96	2.44	New	5b	7.04	-1.13	0.96	4.63	2.15	1.0
Var. <i>RL</i>	6	4.98	-0.79	3.02	4.53	2.13	Var. <i>RL</i>	7	3.8	-12.29	-0.85	18.83	4.34	0.7
Mean	-	3.19	-2.27	0.47	3.03	1.6	Mean	-	6.29	-3.93	0.68	7.76	2.6	-

lifetime prediction to the actual runtime, which is a product of the discharge dynamics. Despite initial large deviations from actual runtime by up to  $-12.29\%$ , the average error over the entire test is found to be only  $-0.85\%$ . This is a bit skewed due to consistently, and significantly underestimating during the first half of the test, which exhibits high dynamics in the load variation. However, for the second half, the mean error is roughly  $1.9\%$  with a maximum and minimum of  $4.52\%$  and  $0.04\%$  respectively.

In summary, especially the rate-discharge and to some extent the recovery effects have a large impact on lifetime prediction when load changes occur. As expected, these effects are less pronounced when a constant load is present. As shown in *Table 4b*, on average the lifetime prediction achieves an accuracy of  $98.05\%$  in the worst case (cold battery) and an impressive  $99.93\%$  in the best case (aged battery).

**Charge Approximation.** Approximation of the *SOC* during the charging process works well under optimal conditions. However, when dealing with real-world conditions where the solar panel’s performance varies due to *e.g.*, clouds, the state machine introduced in *Section 4.3* has difficulties properly tracking the states, which in turn causes the approximation accuracy to suffer. Considering the relatively good performance during discharge, this is not considered an issue for the moment, but will be further investigated.

## 6 Conclusions

This paper presented a light-weight approach to battery state-of-charge approximation that relies fully on closed-loop voltage and optional drain current measurements and does not require any special purpose hardware. Instead it leverages the behavior of the battery under load, which is extracted from discharge traces. Therefore, it incurs only limited implementation effort to adapt for a variety of systems. The proposed approach achieves state-of-charge approximation with over  $95\%$  accuracy even under varying operating conditions. Minimal operational overhead make this approach suitable for a wide variety of low-performance embedded computing systems that leverage off-the-shelf energy harvesting set-ups.

## 7 Acknowledgments

The authors would like to thank their shepherd Leo Selavo for the valuable input. This work was supported by NCCR-MICS, a center funded by the Swiss National Science Foundation under grant number 5005-67322, and the Swiss Nano-Tera.ch initiative.

## References

1. V. Agarwal *et al.*, "Development and Validation of a Battery Model Useful for Discharging and Charging Power Control and Lifetime Estimation," *Energy Conversion, IEEE Transactions on*, vol. 25, no. 3, pp. 821–835, sept. 2010.
2. D. Alessandrelli *et al.*, "ScanTraffic: Smart Camera Network for Traffic Information Collection," in *EWSN'12*, 2012, pp. 196–211.
3. H. J. Bergveld, "Battery management systems : design by modelling," Ph.D. dissertation, Enschede, June 2001.
4. J. Beutel, B. Buchli, F. Ferrari, M. Keller, M. Zimmerling, and L. Thiele, "X-SENSE: Sensing in extreme environments," in *Design, Automation Test in Europe Conference Exhibition (DATE), 2011*, March 2011, pp. 1–6.
5. B. Buchli *et al.*, "Demo abstract: Feature-rich experimentation for wsn design space exploration," in *Proceedings of the 10th International Conference on Information Processing in Sensor Networks (IPSN 2011)*. Chicago, IL, USA: ACM/IEEE, 2011, pp. 115–116.
6. B. Buchli, F. Sutton, and J. Beutel, "GPS-Equipped Wireless Sensor Network Node for High-Accuracy Positioning Applications," in *EWSN'12*, 2012, pp. 179–195.
7. M. Cardei and D.-Z. Du, "Improving wireless sensor network lifetime through power aware organization," *Wirel. Netw.*, vol. 11, no. 3, pp. 333–340, May 2005.
8. A. Castagnetti *et al.*, "An efficient state of charge prediction model for solar harvesting wsn platforms," in *Systems, Signals and Image Processing (IWSSIP), 2012 19th International Conference on*, april 2012, pp. 122–125.
9. Concorde Battery Corporation, *Technical Manual for Lifeline Batteries*, July 2011.
10. D. Doerffel and S. Abu-Sharkh, "A critical review of using Peukert-equation for determining the remaining capacity of lead-acid and lithium ion batteries," *Journal of Power Sources*, vol. 155, no. 2, pp. 395–400, 2006.
11. A. Dunkels *et al.*, "Software-based on-line energy estimation for sensor nodes," in *Proceedings of the 4th workshop on Embedded networked sensors*, ser. EmNets '07. New York, NY, USA: ACM, 2007, pp. 28–32.
12. P. M. Glatz *et al.*, "Designing Perpetual Energy Harvesting Systems explained with RiverMote: A Wireless Sensor Network Platform for River Monitoring," *Electronic Journal of Structural Engineering, Special Issue: Wireless Sensor Networks and Practical Applications*, pp. 55–65, 2010.
13. J. Han *et al.*, "State-of-charge estimation of lead-acid batteries using an adaptive extended Kalman filter," *Journal of Power Sources*, vol. 188, no. 2, pp. 606–612, 2009.
14. J. K. Hart, K. Martinez, R. Ong, A. Riddoch, K. Rose, and P. Padhy, "An autonomous multi-sensor subglacial probe: Design and preliminary results from briksdalsbreen, norway," *Journal of Glaciology*, vol. 51, no. 178, pp. 389–397, 2006.
15. F. B. James M. Gilbert, "Comparison of energy harvesting systems for wireless sensor networks," *International Journal of Automation and Computing*, vol. 5, no. 4, p. 334, 2008.
16. J. Jeong, X. F. Jiang, and D. E. Culler, "Design and Analysis of Micro-Solar Power Systems for Wireless Sensor Networks," EECS Department, University of California, Berkeley, Tech. Rep. UCB/EECS-2007-24, Feb 2007.
17. X. Jiang *et al.*, "Micro power meter for energy monitoring of wireless sensor networks at scale," in *Proceedings of the 6th international conference on Information processing in sensor networks*, ser. IPSN '07. New York, NY, USA: ACM, 2007, pp. 186–195.
18. F. Kerasiotis, A. Prayati, C. Antonopoulos, C. Koulamas, and G. Papadopoulos, "Battery lifetime prediction model for a wsn platform," in *Proceedings of the 2010 Fourth International Conference on Sensor Technologies and Applications*, ser. SENSORCOMM '10. Washington, DC, USA: IEEE Computer Society, 2010, pp. 525–530.
19. Maxim Integrated Products. (1998) Evaluation Kit for the MAX1660. <http://datasheets.maxim-ic.com/en/ds/MAX1660EVKIT.pdf> [Accessed: December 21, 2012].
20. Morningstar Corporation, *SunSaver Photovoltaic System Controllers Operator's Manual*, November 2009.
21. C. Park, K. Lahiri, and A. Raghunathan, "Battery discharge characteristics of wireless sensor nodes: An experimental analysis," in *In Proceedings of the IEEE Conf. on Sensor and Ad-hoc Communications and Networks (SECON)*, 2005.
22. M. T. Penella Lopez *et al.*, "Powering wireless sensor nodes: primary batteries versus energy harvesting," 2009.
23. W. Peukert, "Über die Abhängigkeit der Kapazität von der Entladestromstärke bei Bleiakumulatoren," vol. 18, pp. 287–288, 1897.
24. S. Piller *et al.*, "Methods for state-of-charge determination and their applications," *Journal of Power Sources*, vol. 96, no. 1, pp. 113–120, 2001.
25. V. Pop *et al.*, "State-of-the-art of battery state-of-charge determination," *Measurement Science and Technology*, vol. 16, no. 12, p. R93, 2005.
26. V. Raghunathan *et al.*, "Design considerations for solar energy harvesting wireless embedded systems," in *Information Processing in Sensor Networks, 2005. IPSN 2005. Fourth International Symposium on*, april 2005, pp. 457–462.
27. J. F. Randall. John Wiley & Sons, Ltd, 2006, pp. 1–11.
28. R. Rao, S. Vrudhula, and D. Rakhmatov, "Battery modeling for energy aware system design," *Computer*, vol. 36, no. 12, pp. 77–87, dec. 2003.
29. J. Taneja, J. Jeong, and D. Culler, "Design, modeling, and capacity planning for micro-solar power sensor networks," in *Information Processing in Sensor Networks, 2008. IPSN '08. International Conference on*, april 2008, pp. 407–418.
30. A. Vasebi *et al.*, "A novel combined battery model for state-of-charge estimation in lead-acid batteries based on extended Kalman filter for hybrid electric vehicle applications," *Journal of Power Sources*, vol. 174, no. 1, pp. 30–40, 2007, Hybrid Electric Vehicles.
31. S. Weber *et al.*, "Design and measurement assembly to study in-situ rock damage driven by freezing," in *Proceedings of the Tenth International Conference on Permafrost, Volume 1: International Contributions*, vol. 1. Salekard, Yamal-Nenets autonomous district, Russland: The State Enterprise of the Yamal-Nenets Autonomous District, The Northern Publisher (Severnoye Izdatelstvo), 2012, pp. 437–442.